Available online at www.sciencedirect.com
ScienceDirect
Energy and Buildings 39 (2007) 962–974
ENERGY and BUILDINGS
www.elsevier.com/locate/enbuild

Numerical study on thermal behavior of classical or composite Trombe solar walls

Jibao Shen [a,b], Stéphane Lassue [a,*], Laurent Zalewski [a], Dezhong Huang [b]

[a] *Laboratoire d'Artois de Mécanique Thermique et Instrumentation (LAMTI), Faculté des Sciences Appliquées, Université d'Artois, 62400 Béthune, France*
[b] *Department of Civil Engineering, School of Engineering, Shaoxing College of Arts and Sciences, Shaoxing University, Shaoxing, Zhejiang 312000, China*

Received 21 October 2005; received in revised form 20 November 2006; accepted 21 November 2006

Abstract

It is very difficult to calculate and analyze with precision the thermal behavior of the walls of building envelope when coexist various modes of thermal transfer and because of the particularly random climatic phenomena. These problems are very complex in the case of special components such as passive solar wall used in ''bio-climatic'' architecture. In this paper, the thermal performances of passive solar systems, a classical Trombe wall and a composite Trombe–Michel wall, are studied. The models were developed by our cares with the finite differences method (FDM) [L. Zalewski, S. Lassue, B. Duthoit, M. Butez, Study of solar walls—validating a numerical simulation model, International Review on Building and Environment, 37 (1) (2002) 109–121], and with TRNSYS software [Solar Laboratory of energy (USA), Manuals of TRNSYS, University of Wisconsin-Madison, USA, 1994]. The model for a composite wall developed with FDM was validated by experimentation [1]. The comparisons between the results of simulation with TRNSYS [2] and with FDM, and between the results of simulation a classical Trombe wall and the results of simulation and a composite Trombe wall have been made. They show that the models developed by ourselves are very precise, and the composite wall has better energetic performances than the classical wall in cold and/or cloudy weather.

Keywords: Passive solar system; Solar wall; Classical wall; Composite wall; Finite difference method; TRNSYS

1. Introduction

The passive solar walls collect and store solar energy which can contribute to the heating of buildings. Most known is the classical Trombe wall, passive solar system. A glazing is installed at a small distance from a massive wall. The wall absorbs solar radiation and transmits parts of it into the interior of the building by natural convection through a solar chimney formed by the glazing on one side and the wall on the other. The principal advantage of the classical Trombe wall is its simplicity, but one major problem is its small thermal resistance. If the solar energy received by the wall is reduced, during the night or prolonged cloudy periods, some heat flux is transferred from the inside to the outside, which results in excessive heat loss from the building. This problem becomes important in the regions with cold climates and/or with high latitudes. A solution is to use a composite Trombe–Michel wall [7] which includes an insulating layer. Zrikem and Bilgen [3], Zalewski [4].

It is rather difficult to establish a general rule to calculate with precision the capacity of storage and of energy recuperation of solar energy for this sort of wall. It is necessary for that to resort to simulation tools such as TRNSYS developed by the members of US Solar Energy Laboratory at the University of Wisconsin-Madison. Thanks to the component Type 36 of TRNSYS, we can easily study the classical Trombe wall. To study the composite Trombe–Michel wall, we designed a new simulation component.

In this work, the classical and composite wall systems are studied and the finite differences method is used. In the following section, the thermal study of a classical wall and a composite wall, the comparisons of the simulation results by TRNSYS and those of simulation with the finite difference method (FDM) are presented. The comparisons between both walls are also presented.

* Corresponding authors at: Laboratoire d'Artois de Mécanique Thermique et Instrumentation (LAMTI), Faculté des Sciences Appliquées, Université d'Artois, 62400 Béthune, France. Tel.: +33 3 21 63 71 54; fax: +33 3 21 63 71 23.
E-mail addresses: articlejbs2004@yahoo.com.cn (J. Shen), lassue@univ-artois.fr (S. Lassue), laurent.zalewski@univ-artois.fr (L. Zalewski).

0378-7788/$ – see front matter © 2006 Elsevier B.V. All rights reserved.
doi:10.1016/j.enbuild.2006.11.003

Nomenclature

a	thermal diffusivity (m^2/s)
A	area (m^2)
C	specific heat (J/kg °C)
C_d	discharge coefficient
D	distance (m)
g	acceleration of gravity (m/s^2)
Gr	Grashof number
h_e	convection coefficient (W/m^2 °C)
h_r	radiation coefficient (W/m^2 °C)
H	height (m)
H_o	vertical distance between two vents (m)
I_g	global solar radiation flux density (W/m^2)
I_d	diffuse solar radiation flux density (W/m^2)
I_h	solar radiation flux density on a horizontal surface (W/m^2)
L	width (m)
m	air mass flow rate (kg/s)
Nu	Nusselt number
Pr	Prandtl number
Q	thermal energy (J)
Ra	Rayleigh number
t	time (s)
T	temperature (°C)
T_{abs}	temperature (K)
V	fluid velocity (m/s)
x, z	Cartesian coordinates
X	thickness (m)

Greek letters

α	solar absorptivity
β	thermal expansion coefficient (K^{-1})
ε	emissivity
ζ	sum of load loss coefficients
λ	thermal conductivity (W/m °C)
μ	dynamic viscosity (kg/m s)
ρ	density (kg/m^3)
σ	Stefan–Boltzmann constant (5.674×10^{-8} W/m^2 K^4)
τ	transmissivity
φ	heat flux density (W/m^2)
Φ	heat flux (kJ/h)

Subscripts

abs	absolute temperature
am	ambiance
c	convection
e	emission
e	exterior
env	environment
f	fluid
g	glazing
gy	gypsum
i	insulating
int	interior (dwelling)
m	massive wall
o	orifice of ventilation (vent)
r	radiation
s	solar
sf	surface

In this work, the meteorological data used are the one from Carpentras in south of France (latitude 44.05°N, longitude 5.03°E). The parameters of the composite wall are based on a previous experimental study Zalewki and coworkers [4,5]. To compare both walls, some parameters of the classical wall are based on that of the experimental composite wall. With the component Type 36 of TRNSYS, we consider only one layer for the massive wall (the layer of gypsum is not considered for simulations of the classical wall). It will be assumed that the thermal exchange exists in only one direction only and there are no heat losses in the others.

2. Classical Trombe wall

2.1. Functioning principle

The classical Trombe wall is constituted of a massive wall installed at a small distance from a glazing. In the case of the thermo-circulation phenomenon, the massive wall absorbs the solar flux through the glazing(s). The wall transfers a part of the flux inside the building by conduction. The heating of the air in contact with this wall induces a natural circulation: the air is admitted by the lower vent of the wall and comes back to the room by the upper vent. The air circulating, transfers part of the solar heat flux (cf. left part of Fig. 1).

An inverse thermo-siphon phenomenon was observed at the time of little or non-sunny periods at night or in winter. In fact, when the wall becomes colder than the indoor temperature, an air circulation, from the vent on top to the vent at the bottom, produces itself and comes to cool the habitat. To resolve this problem, we can, for example, place a supple plastic film at the level of the orifices, when there is a thermo-siphon phenomenon. The vents are then opened, and in the opposite case they are closed.

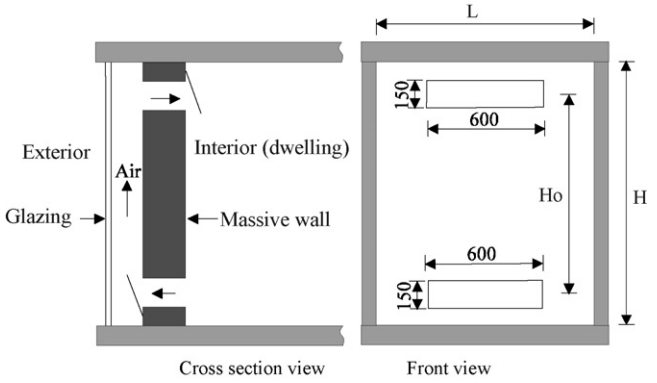

Fig. 1. Classical Trombe wall.

2.2. Description of the classical Trombe wall for studying

We choose to compare the results of TRNSYS simulation with those of simulation by FDM. The parameters of the wall based on a previous experimental study of the composite wall Zalewski [4]. The geometric characteristics of the classical Trombe wall studied are illustrated in Fig. 1.

The wall studied has the following characteristics:

(1) Azimuth surface angle of the wall, $\gamma = 0$ (South orientation).
(2) Wall height, $H = 2.47$ m.
(3) Wall width, $L = 1.34$ m.
(4) Massive wall thickness, $X = 0.15$ m.
(5) Massive wall conductivity, $\lambda_m = 0.8117$ W/(m °C).
(6) Thermal capacity of the massive wall, $\rho_m C_m = 1.803 \times 10^6$ J/(m^3 °C) ($\rho_m = 1900$ kg/m^3, $C_m = 949$ J/kg °C).
(7) Solar absorption of the massive wall, $\alpha = 0.9$.
(8) Emissivity of the massive wall, $\varepsilon_m = 0.9$.
(9) Emissivity of the glazing, $\varepsilon_g = 0.9$.
(10) Number of glazing, $N_g = 1$.
(11) Distance between the surface of the glazing and one of the massive wall, $D = 0.03$ m.
(12) Surface of the massive wall vent, $A_o = 0.15 \times 0.60 = 0.09$ m^2.
(13) Vertical distance between two vents, $H_o = 2.15$ m.
(14) Temperature of the dwelling, $T_{int} = 19$ °C (constant).
(15) Global exchange coefficient (by convection and by radiation) between the surface of the massive wall and the dwelling, $h_{int} = h_{r\ int} + h_{c\ int} = 9.1$ W/(m^2 °C).
(16) Transmissivity of the glazing, $\tau = 0.81$.

2.3. Analysis of the different thermal exchanges

The analysis of the different thermal exchanges for the classical wall is similar to that for the composite wall presented in the next section. The analogical diagram of the thermal heat transfer in the classical wall is shown in Fig. 2.

The Type 36 of TRNSYS uses only one parameter for the height of the wall and the distance between two vents, and one layer for the massive wall. Since the air mass flow rate in the chimney formed by the glazing and the massive wall flows between two openings of ventilation, we only considered the wall surface between these two vents ($H = 2.15$ m, $L = 1.34$ m).

3. Composite Trombe–Michel wall

3.1. Functioning principle

The functioning of a composite Trombe–Michel wall is similar to that of a classical Trombe wall. But the latter induces important heat loss during the cold periods due to the small thermal resistance of the massive wall. We can remedy this problem while using the composite wall. The latter has an insulating wall at the back of the massive wall. The thermal energy can be transferred from outside to the interior air layer

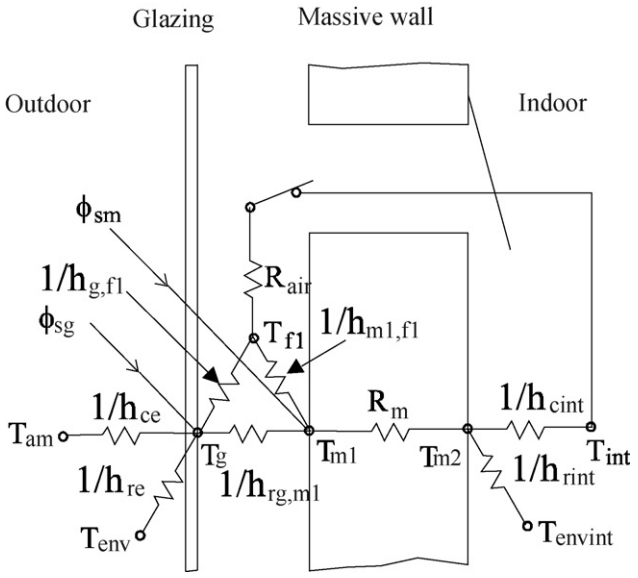

Fig. 2. Analogical diagram of classical Trombe wall.

by conduction in the massive wall. Then it can be transferred by convection while using the thermo-circulation phenomenon of air between the massive wall and the insulating wall. At the time of little or non-sunny days during winter or at nights, the vents in the insulating wall are closed. Thanks to the big thermal resistance, there is little thermal flux that going from indoor to outdoor (little loss) (cf. Fig. 3).

This passive solar wall has been studied experimentally within the framework of Zalewski's [4]. The measurements were realized on the Cadarache site in the south of France and made possible to set up a simulation model based on the use of the finite difference method FDM.

Simultaneous measurements of heat fluxes and of surface temperatures particularly at the level of the massive wall have allowed us to quantify the energetic performances of this component and to validate our simulation model within the framework of an experimental follow up which lasted several years.

For example one can observe the good correspondence between the heat flows measured and simulated in Fig. 4, here during a week in winter.

This model made possible to position the composite Trombe wall as regards the more classical walls in terms of energetic balance for heating period (1/10 to 20/05, see Fig. 5).

3.2. Description of the composite Trombe–Michel wall for studying

We chose the parameters of the composite Trombe–Michel wall according to the previous experimental study Zalewski and coworkers [4,5]. The geometric characteristics of the wall studied are illustrated by Fig. 3.

The wall exposed to the south has the following characteristics:

(1) Wall height, $H = 2.47$ m.

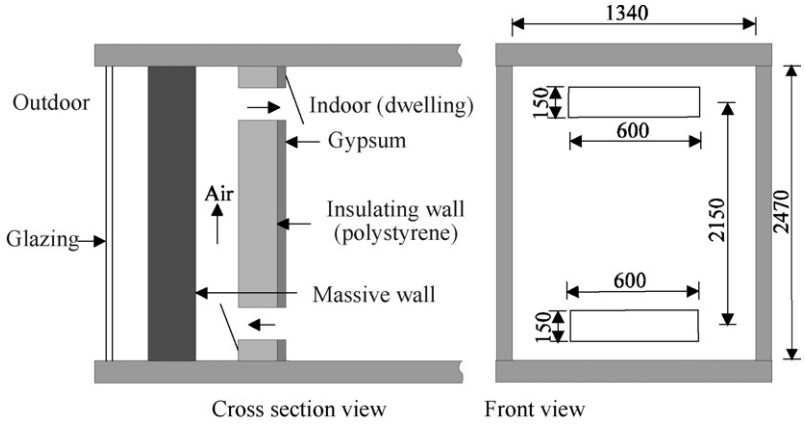

Fig. 3. Composite Trombe–Michel wall.

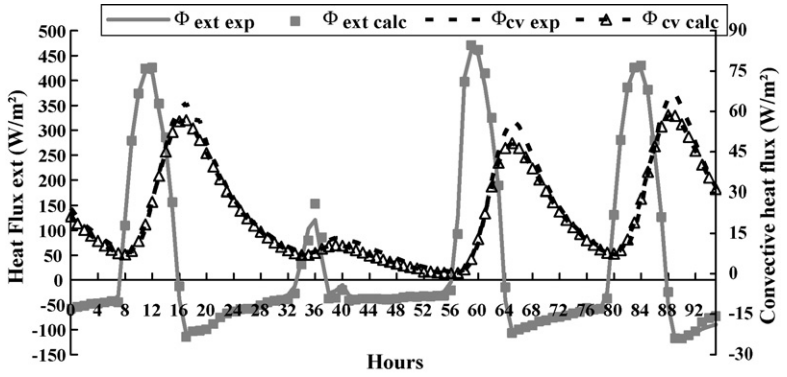

Fig. 4. Comparison between experimentation and numerical simulation [1,4].

(2) Wall width, $L = 1.34$ m.
(3) Emissivity of the glazing, $\varepsilon_g = 0.9$.
(4) Interval between the surface of the glazing and that of the massive wall, $D_1 = 0.03$ m.
(5) Massive wall thickness, $X_1 = 0.15$ m.
(6) Conductivity of the massive wall, $\lambda_m = 0.8117$ W/(m °C).
(7) Thermal storage capacity of the massive wall, $\rho_m C_m = 1.803 \times 10^6$ J/(m^3 °C) ($\rho_m = 1900$ kg/m^3, $C_m = 949$ J/kg °C).
(8) Solar absorption of the massive wall, $\alpha = 0.9$.
(9) Emissivity of the massive wall, $\varepsilon_m = 0.9$.

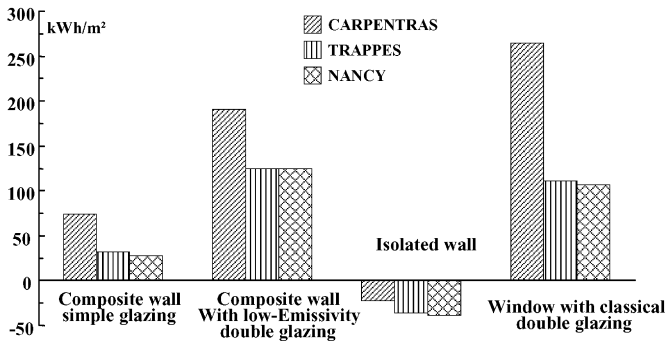

Fig. 5. Energetic performances.

(10) Interval between the surface of the massive wall and that of the insulating wall, $D_2 = 0.04$ m.
(11) Height of the vents of the insulating wall, $H'_o = 0.15$ (m).
(12) Width of the vents of the insulating wall, $L_o = 0.6$ m.
(13) Vertical distance between two vents, $H_o = 2.15$ m.
(14) Insulating wall thickness, $X_2 = 0.075$ m.
(15) Conductivity of the insulating wall, $\lambda_i = 0.041$ J/(s m °C).
(16) Thermal storage capacity of the insulating wall, $\rho_i C_i = 24{,}000$ J/(m^3 °C) ($\rho_i = 30$ kg/m^3, $C_i = 800$ J/kg °C).
(17) Emissivity of the insulating wall, $\varepsilon_i = 0.6$.
(18) Gypsum thickness, $X_{gy} = 0.01$ m.
(19) Conductivity of gypsum, $\lambda_{gy} = 0.2575$ W/(m °C).
(20) Thermal storage capacity of gypsum, $\rho_{gy} C_{gy} = 8 \times 10^5$ W/(m^3 °C) ($\rho_{gy} = 1000$ kg/m^3, $C_{gy} = 800$ J/kg °C).
(21) Emissivity of gypsum, $\varepsilon_{gy} = 0.9$.
(22) Transmissivity of the glazing, $\tau = 0.81$.
(23) Indoor temperature, $T_{int} = 19$ °C (constant).

3.3. Study and characterization of the different thermal exchanges

The analogical diagram of the thermal heat transfer in a composite Trombe–Michel wall [7] is represented in Fig. 6.

We will analyze the composite wall as follows: T_f is the average air temperature in °C and T_{fabs} is the average absolute air temperature in Kelvin.

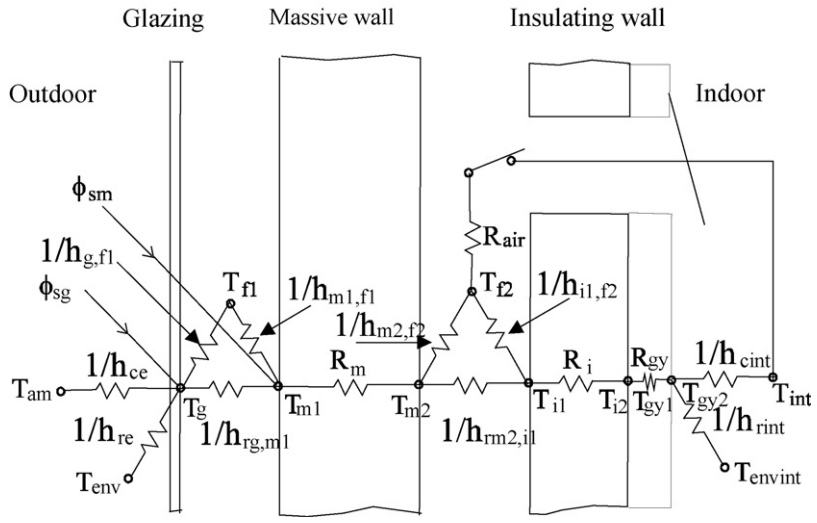

Fig. 6. Analogical thermal diagram of composite Trombe–Michel wall.

We assume that the thermal conductivity λ_f of the fluid, density ρ_f and the thermal expansion coefficient β_f are functions of the temperature:

$$\lambda_f = C_1 + C_2 T_{f\,abs}\,(W/m\,^\circ C) \quad (C_1 = 0.01029096; C_2 = 0.000281592), \qquad \rho_f = \frac{\rho_{ref}}{T_{f\,abs}} \quad (\rho_{ref} = 341.8), \qquad \beta_f = \frac{1}{T_{f\,abs}}$$

(a) Between outdoor and the massive wall:

(a.1) Exchange coefficients on the exterior surface of the glazing;

For the natural convection on the outside surface of a glazing, we have approximated the convection coefficient by Mc Adams [4,8,10,11]:

$$h_{ce} = 5.7 + 3.8 V_{wind}\,(W/m^2\,^\circ C)$$

where V_{wind} is the average wind velocity in m/s.

And the radiation coefficient on the outside surface of a glazing:

$$h_{re} = \sigma \varepsilon_g (T^2_{env\,abs} + T^2_{g\,abs})(T_{env\,abs} + T_{g\,abs})$$

where $T_{env\ abs}$ is the environment temperature (sky) in K and $T_{g\ abs}$ is the temperature of the glazing in K.

(a.2) Energy balance on the glazing:

The thermal balance on the glazing is written as follows:

$$\phi = h_{ce}(T_{am} - T_g) + h_{re}(T_{env} - T_g) + \phi_{sg} = \left(\frac{h_{rg,m1} + h_{g,f1}}{2}\right)(T_g - T_{m1})$$

where T_{am} is the air ambient temperature, φ_{sg} the solar flux absorbed by the glazing, $h_{rg,m1}$ the radiation coefficient on the inside surface of the glazing, and $h_{g,f1}$ is the convection coefficient on the inside surface of the glazing.

$h_{rg,m1}$ is determined by

$$h_{rg,m1} = \sigma F_{eg,m1}(T^2_{g\,abs} + T^2_{m1\,abs})(T_{g\,abs} + T_{m1\,abs})$$

where $F_{eg,m1} = 1/((1/\varepsilon_g) + (1/\varepsilon_m) - 1)$ is the emission factor between the inside surface of the glazing and the outside surface of the massive wall, $T_{g\,abs}$ the temperature of the glazing in K, $T_{m1\,abs}$ is the temperature of the inside surface of the massive wall in K.

$h_{g,f1}$ is determined by

$$h_{g,f1} = \frac{Nu\lambda_{f1}}{D_1}$$

The average temperature of the fluid: $T_{f1} = (T_{m1} + T_g)/2$.

The Nusselt number Nu is defined according to the correlation of Raithby and coworkers [6,9,10,13]:

$$Nu = \mathrm{Max}\{1, 0.288(Ra/K_A)^{0.25}, 0.039Ra^{0.33}\},$$

Rayleigh number, $Ra = GrPr$, Grashof number,

$$Gr = \frac{\beta_{f1} g \rho^2_{f1} D^3_1 (T_{m1} - T_{f1})}{\mu^2},$$ Prandtl number,

$$Pr = \frac{\mu C_{f1}}{\lambda_{f1}}$$

Aspect factor $K_A = H/D_1$ (ratio between the wall height and the interval between two planes (glazing − massive wall)).

(a.3) Energy balance on the outside surface of the massive wall:

The boundary condition is obtained from the equation of the energy balance on the outside surface of the wall:

$$-\lambda_m \left.\frac{\partial T}{\partial x}\right|_{x=0} = \left(\frac{h_{rg,1} + h_{g,f1}}{2}\right)(T_g - T_{m1}) + \phi_{sm}$$

where φ_{sm} is the solar heat flux absorbed by the massive wall.

(b) In the massive wall (conduction):

The thermal flux through the massive wall is determined by the one-dimensional equation:

$$\frac{\partial T}{\partial t} = a_m \frac{\partial^2 T}{\partial x^2} \quad (0 < x < X1)$$

a_m is the diffusivity of the massive wall, $a_m = \lambda_m/\rho_m C_{pm}$.

(c) Between the massive wall and the insulating wall:

(c.1) Radiation coefficient:

The radiation coefficient between the inside surface of the massive wall and the outside surface of the insulating wall:

$$h_{rm2,i1} = \sigma F_{em2,i1}(T^2_{m2\,abs} + T^2_{i1\,abs})(T_{m2\,abs} + T_{i1\,abs})$$

where $F_{em2,\,i1} = 1/((1/\varepsilon_m) + (1/\varepsilon_i) - 1)$ is the emission factor between the inside surface of the massive wall and the outside surface of the insulating wall, $T_{m2\,abs}$ the temperature on the inside surface of the massive wall in K, and $T_{i1\,abs}$ is the temperature on the outside surface of the insulating wall in K.

(c.2.) Air mass flow in the chimney—load losses (case of the open vents).

(c.2.1) Air mass flow rate.

The flow in the chimney is produced naturally by the thermo-siphon. The thermal resistance between the inside surface of the massive wall and the outside surface of the insulating wall, depends on the air mass flow through the opening vents in the insulating wall. In our case this thermal resistance is calculated on the assumption that all the load losses are caused by the upper and lower air vent.

The air mass flow in the chimney is produced between two vents, so we only considered the wall section between these vents ($H_o = 2.15$ m, $L = 1.34$ m).

We suppose that the air temperature in the chimney varies linearly along the chimney height. The air average temperature in the space between the inside surface of the massive wall and the "outside" surface of the insulating wall will therefore be

$$T_{f2} = \frac{(T_{o\,bottom} + T_{o\,top})}{2}$$

where $T_{o\,top}$ is the air temperature in the upper vent and $T_{o\,bottom}$ is the air temperature in the lower vent.

The air mass flow is directly linked to the difference of the air temperatures existing between the vents, and equally to the sum of the load losses produced during the air flow crossing the chimney (i.e. Idel'cik [14]).

The global load loss ΔH, sum of load losses by friction and the load losses unique, is equal to

$$\Delta H = \zeta \frac{\gamma_{f2} V^2_{f2}}{2g}$$

where ζ is the sum of the load losses coefficients, γ_{f2} the average specific weight of the air in the chimney, and V_{f2} is the average velocity of the air mass flow in the chimney.

While assuming the air to be perfect gas, admitting the hypothesis of a permanent flow and following the one-dimensional vertical one (z), and neglecting the viscosity effects, we obtain the load loss between the entry (lower vent) and the exit of the canal (upper vent):

$$\Delta H = \int_0^{H_o} \gamma \, dz$$

where H_o is the vertical distance between the orifices.

While supposing that the temperature varies linearly on the journey of the air along the wall, from the two preceding relations, we deduce the speed of the air in the chimney:

$$V_{f2} = C_d \sqrt{\frac{g H_o (T_{o\,top\,abs} - T_{o\,bottom\,abs})}{T_{o\,top\,abs} + T_{o\,bottom\,abs}}}$$

where $C_d = \sqrt{2/\zeta}$ is the discharge coefficient, $T_{o\,top\,abs}$ the air temperature at the upper vent in K, and $T_{o\,bottom\,abs}$ is the air temperature at the lower vent in K.

The sum of the load loss coefficients is determined by

$$\begin{aligned}\zeta = {} & \zeta_{linear} + \zeta_{entry} \frac{\rho_{f2}}{\rho_{fl}} \left(\frac{A_{chim}}{A_o}\right)^2 \\ & + \zeta_{out} \frac{\rho_{f2}}{\rho_{fo}} \left(\frac{A_{chim}}{A_o}\right)^2 \\ & + \zeta_{o\,bottom} \frac{\rho_{f2}}{\rho_{fl}} \left(\frac{A_{chim}}{A_o}\right)^2 \\ & + \zeta_{o\,top} \frac{\rho_{f2}}{\rho_{fo}} \left(\frac{A_{chim}}{A_o}\right)^2 \\ & + \zeta_{elbow\,.bottom} \frac{\rho_{f2}}{\rho_{fl}} \left(\frac{A_{chim}}{A_o}\right)^2 + \zeta_{elbow\,top}\end{aligned}$$

where A_{chim}/A_o is the ratio between the chimney section and that of the orifices, ρ_{f2} the density at the average temperature T_{f2}, ρ_{fl} the density at the average temperature $T_{o\,bottom}$, ρ_{fo} the density at the average temperature $T_{o\,top}$, ζ_{linear} the linear load loss in the chimney, ζ_{entry} the load singular loss coefficient at the entry, ζ_{out} the load loss coefficient at the exit (rush expansion), ζ_o the load loss coefficient at the level of the orifices ($\zeta_{o\,bottom}$ and $\zeta_{o\,top}$), and

ζ_{elbow} is the load loss coefficient at the level of the elbows ($\zeta_{elbow\ bottom}$ and $\zeta_{elbow\ top}$).

Here, the coefficients ζ_{elbow} depends on the dimensions of the chimney, its orifice, on the angle of the elbows, and also on the nature of the materials. If the device contains a ''dead'' zone in the ventilated air layer upon the upper vent, the coefficient ζ_{elbow} must be increased by 20% [14].

It is therefore possible to calculate the air mass flow rate m in the chimney as follows:

$$\frac{m}{\rho_{f2}} = C_d A \sqrt{\frac{g H_o (T_{o\,abs} - T_{i\,abs})}{T_{o\,abs} + T_{i\,abs}}}$$

Then the air mass flow is calculated by the following formula:

$$m = \rho_{f2} C_d A \sqrt{\frac{g H_o (T_{o\,top\,abs} - T_{o\,bottom\,abs})}{T_{o\,top\,abs} + T_{o\,bottom\,abs}}}$$

(c.2.2) Thermal balance in the chimney (convection)

The thermo-circulation is produced when the average temperature in the chimney is higher than that of the indoor temperature.

The thermal energy transported by the air towards the top orifice is written as

$$\phi_o = \frac{m C_{f2} (T_{o\,top} - T_{o\,bottom})}{A_m} = h_{m2,f2}(T_{m2} - T_{f2}) + h_{i1,f2}(T_{i1} - T_{f2})$$

where $h_{m2,f2}$ is the convection coefficient at the inside surface of the massive wall and $h_{i1,f2}$ is the convection coefficient at the outside surface of the insulating wall.

$h_{m2,f2}$, $h_{i1,f2}$ are determined by

$$h_{m2,f2} = h_{i1,f2} = \frac{Nu \lambda_{f2}}{H_o}$$

The Nusselt number is defined according to the correlation of Fishenden and Saunders [3,15]:

$$Nu = 0.107 Gr^{1/3}$$

The Grashof number is defined as follows:

$$Gr = \frac{\beta_{f2} g \rho_{f2}^2 H_o^3 (T_{o\,top} - T_{o\,bottom})}{\mu^2}$$

(c.2.3) Energy balance on the inside surface of the massive wall:

The boundary condition is obtained from the equation of the energy balance on the inside surface of the wall:

$$-\lambda_m \left.\frac{\partial T}{\partial X}\right|_{x=x1} = h_{m2,f2}(T_{m2} - T_{f2}) + h_{rm2,i1}(T_{m2} - T_{i1})$$

(c.2.4) Energy balance on the outside surface of the insulating wall:

The boundary condition is obtained from the equation of the energy balance on the outside surface of the insulating wall:

$$-\lambda_i \left.\frac{\partial T}{\partial X}\right|_{x=0} = h_{i1,f2}(T_{f2} - T_{m2}) + h_{rm2,i1}(T_{m2} - T_{i1})$$

(c.3) Case in which the vents are closed:

(c.3.1) Energy balance on the inside surface of the massive wall:

The boundary condition is obtained from the equation of the energy balance on the inside surface of the wall:

$$-\lambda_m \left.\frac{\partial T}{\partial X}\right|_{x=x1} = (h_{m2,i1} + h_{rm2,i1})(T_{m2} - T_{i1})$$

(c.3.2) Energy balance on the outside surface of the insulating wall:

The boundary condition is obtained from the equation of the energy balance on the outside surface of the insulating wall:

$$-\lambda_i \left.\frac{\partial T}{\partial X}\right|_{x=0} = (h_{m2,i1} + h_{rm2,i1})(T_{m2} - T_{i1})$$

(c.3.3) Convection coefficient:

$$h_{m2,i1} = \frac{h_{m2,f2}}{2} = \frac{h_{i1,f2}}{2}$$

$h_{m2,f2}$ is determined by

$$h_{m2,f2} - \frac{Nu \lambda_{f2}}{D_2}$$

The Nusselt number Nu is defined according to the correlation of Raithby and coworkers [6,9,10,13]:

$$Nu = \mathrm{Max}\{1, 0.288(Ra/K_A)^{0.25}, 0.039 Ra^{0.33}\},$$

Rayleigh number, $Ra = GrPr$,

Grashof number, $Gr = \frac{\beta_{f2} g \rho_{f2}^2 D_2^3 (T_{m2} - T_{f2})}{\mu^2}$,

Prandtl number, $Pr = \frac{\mu C_{f2}}{\lambda_{f2}}$

$K_A = H/D_2$ is the ratio between the wall height and the two planes' interval.

(d) In the insulating wall (heat conduction):

The thermal flux through the insulating wall is determined by the one-dimensional equation:

$$\frac{\partial T}{\partial t} = a_i \frac{\partial^2 T}{\partial X^2} \quad (0 < X < X_2)$$

a_i is the diffusivity of the insulating wall, $a_i = \lambda_i/\rho_i C_{pi}$.

(e) On the interface between the insulating wall and gypsum:

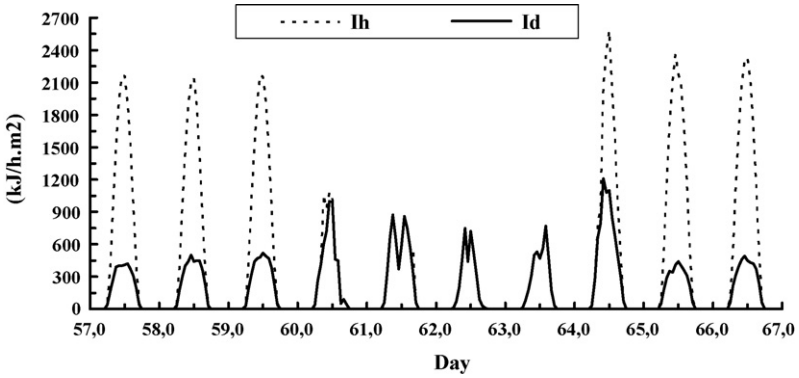

Fig. 7. Meteorological data: solar horizontal heat flux, I_h; solar diffuse heat flux, I_d.

The thermal flux is determined by the equation:

$$\frac{\partial T}{\partial t} = a_{i\,gy}\frac{\partial^2 T}{\partial X^2} \quad (-\delta x < X < \delta x)$$

$a_{i\,gy}$ is the average diffusivity of the insulation material and the gypsum and δx is a small element.

(f) On the inner surface of the insulating wall (on the surface of the gypsum):

The boundary condition is obtained from the equation of energy balance on the inside surface of the wall:

$$-\lambda_{gy}\left.\frac{\partial T}{\partial X}\right|_{x=x2} = h_{int}(T_{gy2} - T_{int})$$

with $h_{int} = h_{r\,gy2} + h_{c\,gy2}$.

The radiation coefficient on the inside surface of the insulating wall towards the heated room:

$$h_{r\,gy2} = \sigma\varepsilon_{gy2}(T_{gy2\,abs}^2 + T_{int\,abs}^2)(T_{gy2\,abs} + T_{int\,abs})$$

The convection coefficient on the inside surface of the insulating wall:

$$H_{c\,gy2} = \frac{Nu\lambda_{f2}}{H_i}$$

where H_i is the insulating wall height.

For the calculation of the coefficient $h_{c\,gy2}$, we use the correlations proposed by the ASHRAE in natural convection for vertical plates [12,16]:

$$\text{if } 10^4 < Gr_H < 10^8, \quad Nu_H = 0.516Ra_H^{1/4}, \quad \text{if } 10^8 < Gr_H < 10^{12}, \quad Nu_H = 0.117Ra_H^{1/3}, \quad \text{Rayleigh number}, Ra_H = Gr_H Pr, \quad \text{Grashof number}, Gr_H = \frac{\beta_{fi} g \rho_{fi}^2 H_i^3 (T_{gy2} - T_{int})}{\mu^2}, \quad \text{Prandtl number}, Pr = \frac{\mu C_{f\,int}}{\lambda_{f\,int}}$$

4. Meteorological data

We have carried out the simulations of the classical Trombe wall and the composite Trombe–Michel wall for 10 days (from the 57th to the 66th day, i.e. from February 26 to March 7). The meteorological data are shown in Figs. 7 and 8. During the first day, there was a lot of sunlight, the horizontal solar flux I_h is big. After 3 days, there were a lot of clouds, the temperature of the air T_{am} went down, and the velocity of the wind V_{wind} raised. During the last day of this period, there was a lot of sun, the horizontal solar flux I_h raised.

5. Comparison of the results of simulations with TRNSYS and FDM

We carried out the simulations of the solar walls with TRNSYS and with the finite differences method (FDM). The

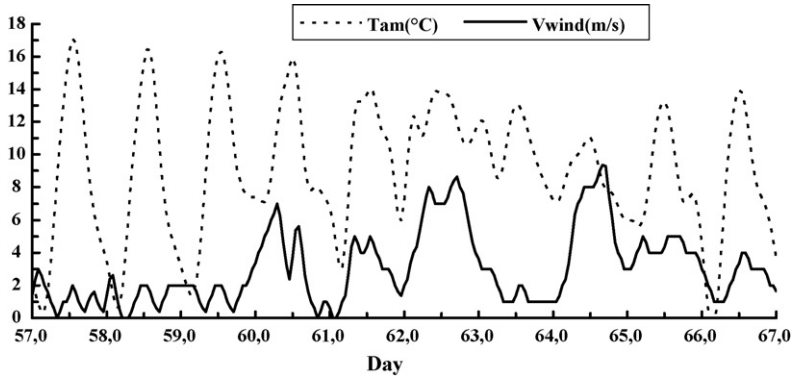

Fig. 8. Meteorological data: outdoor air temperature, T_{am}; velocity of the wind, V_{wind}.

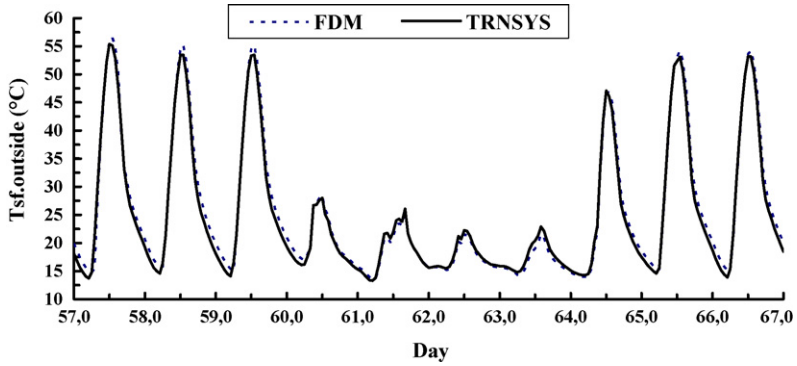

Fig. 9. Comparison of the temperature $T_{\text{sf outside}}$ on the outside surface of the massive wall in the classical wall.

model with FDM had been validated in comparison with experimental results in the case of the composite wall and then modified in order to simulate the functioning of the classical wall Zalewski [4]. In this section, we will compare the simulation results of both methods. It means that we consider the wall without insulation and with air circulation through the massive concrete wall (classical Trombe wall).

5.1. Comparison on the classical wall

Figs. 9–11 indicate the temperature $T_{\text{sf outside}}$ on the outside surface of the massive wall, the temperature $T_{\text{sf inside}}$ on the inside surface of the massive wall and the temperature T_{o} of the air in the upper vent in the classical wall.

Figs. 12 and 13 indicate the thermal flux Φ_{o} transferred from the ventilated air layer to the dwelling and the thermal flux $\Phi_{\text{sf inside}}$ transferred from the inside surface of the massive wall to the dwelling in the classical wall.

In the simulations with TRNSYS, the Type 36 uses the constant global coefficient h_{int}. In reality, h_{int} increases with the temperature difference between the surface and the fluid. Therefore, the temperatures $T_{\text{sf inside}}$ obtained by the two methods are different (see Fig. 10). On the other hand, $T_{\text{sf inside}}$ is a little lower when h_{int} increases. The heat flux $\Phi_{\text{sf inside}}$ is almost the same (see Fig. 13).

The discharge coefficient C_{d} is constant in the simulations with TRNSYS. The discharge coefficient C_{d} is determined by the equation:

$$C_{\text{d}} = \sqrt{\frac{2}{\zeta}}$$

where ζ is the sum of the load loss coefficients:

$$\zeta = C_1 \left(\frac{A_{\text{chim}}}{A_{\text{o}}} \right)^2 + C_2 \quad (C_1 = 8, C_2 = 4)$$

where $A_{\text{chim}}/A_{\text{o}}$ is the ratio of the chimney area to that of the orifices, representing the load loss. The discharge coefficient C_{d} is supposed to be constant.

Contradictory, the discharge coefficient is not constant. It changes with the air speed in the chimney V_{f}. When the solar heat flux I_{h} increases, the temperature $T_{\text{sf outside}}$ on the outside surface of the wall increases with it. And when the speed V_{f} increases, the discharge coefficient C_{d} increases. Therefore, the heat flux Φ_{o} increases. In the simulations with TRNSYS, since C_{d} is constant, the amplitudes of Φ_{o} are smaller (see Fig. 12).

5.2. Comparison on the composite wall

Figs. 14–16 indicate the temperature $T_{\text{sf outside}}$ of the outside surface of the massive wall, the temperature $T_{\text{sf inside}}$ of the inside surface of the insulating wall and the temperature T_{o} of the air in the wall top orifice in the composite wall.

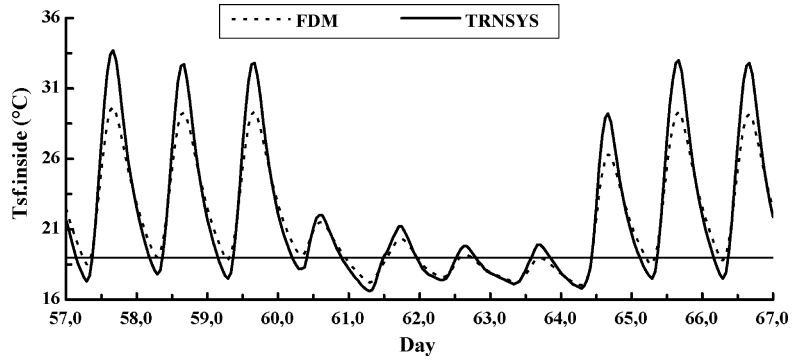

Fig. 10. Comparison of the temperature $T_{\text{sf inside}}$ on the inside surface of the massive wall in the classical wall.

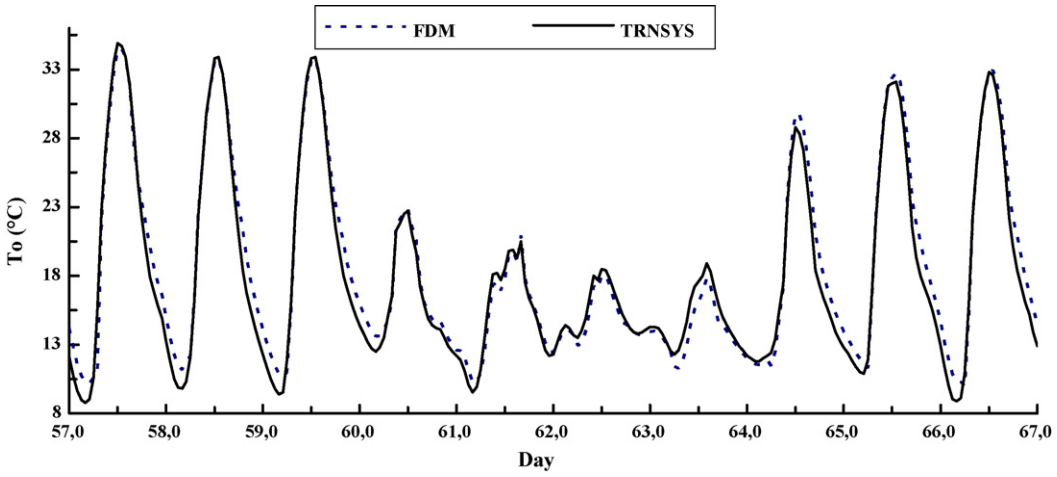

Fig. 11. Comparison of the temperature T_o of the air at the upper vent in the classical wall.

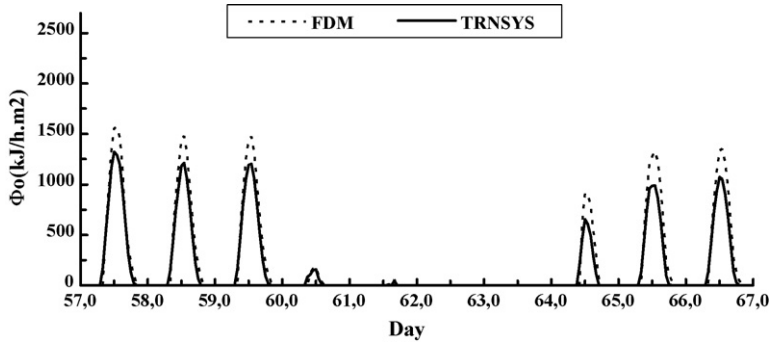

Fig. 12. Comparison of the thermal flux Φ_o in the classical wall.

Fig. 17 indicates the thermal flux Φ_o from the ventilated air layer to the dwelling in the composite Trombe wall.

To calculate the solar flux with TRNSYS, we used the Type 16 (Solar Radiation Processor) TRNSYS manual [2]. But with FDM, we used another method describe by [13,14].

Because of the different calculations, the global solar flux on the vertical wall in the simulation with FDM is a little bigger than that in the simulation with TRNSYS. We can notice that the results in the simulation with FDM are a little bigger than that in the simulation with TRNSYS. Figs. 14–17 shows that the results of the two methods are again very similar. The simulations with TRNSYS for the composite wall seem successful.

6. Comparison between the two walls

We will make comparisons between the two types of walls (see Figs. 18–22).

According to the figures, we note that, every day, the amplitudes of the values for the composite wall are smaller than those for the classical wall.

For the classical wall, at the time of day when it is not very sunny, the minimum $T_{sf\ inside}$ is inferior to T_{int} by 2 °C while on sunny day, the maximum $T_{sf\ inside}$ is more than 26 °C. For the composite wall, the difference between $T_{sf\ inside}$ and T_{int} is less than 1 °C.

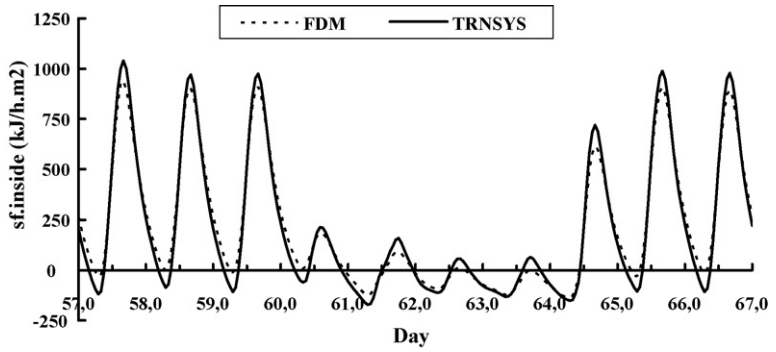

Fig. 13. Comparison of the thermal flux $\Phi_{sf\ inside}$ in the classical wall.

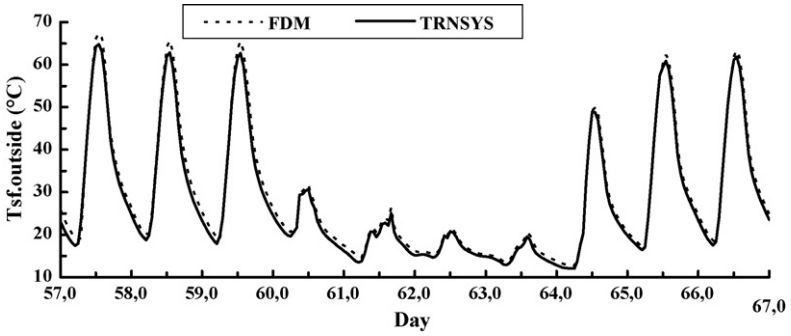

Fig. 14. Comparison of the temperatures $T_{\text{sf outside}}$ on the outside surface of the massive wall in the composite wall.

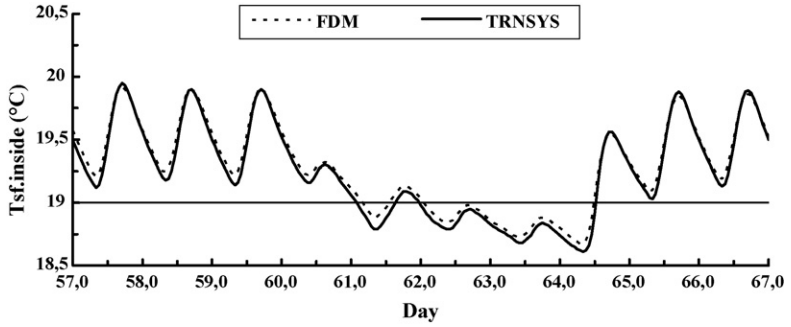

Fig. 15. Comparison of the temperatures $T_{\text{sf inside}}$ on the inside surface of the insulating wall in the composite wall.

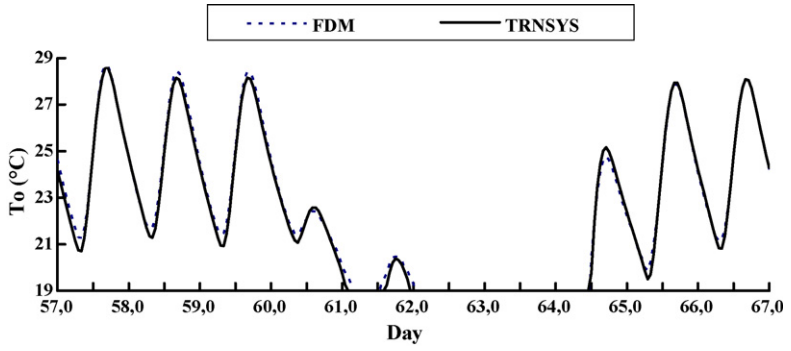

Fig. 16. Comparison of the temperatures T_{o} of the air at the upper vent in the composite Trombe wall.

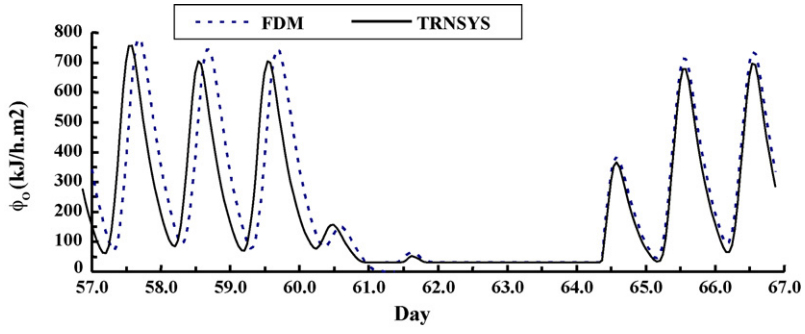

Fig. 17. Comparison of the thermal flux Φ_{o} in the composite wall.

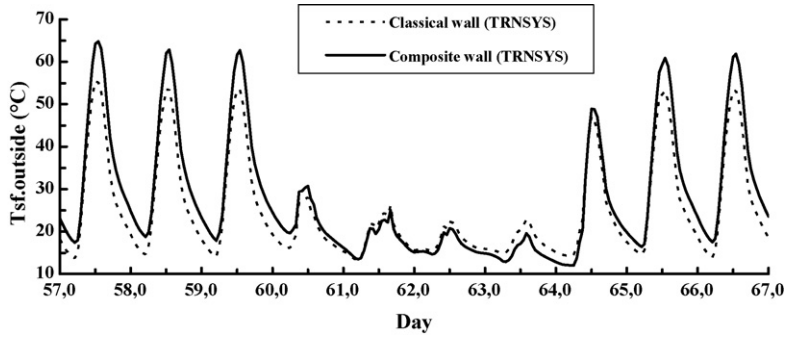

Fig. 18. Comparison of the temperatures $T_{\text{sf outside}}$ of the outside surface of the massive wall.

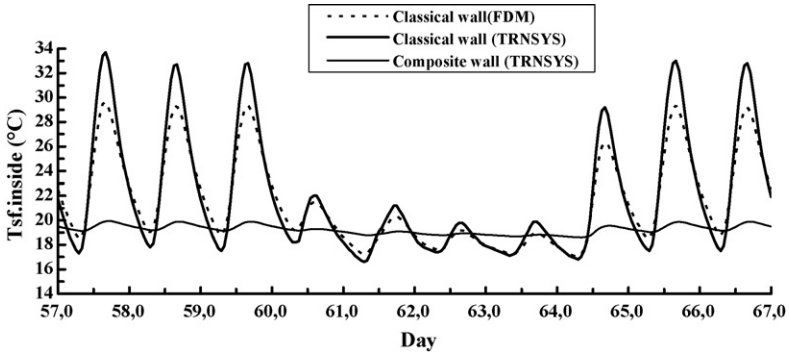

Fig. 19. Comparison of the temperature $T_{\text{sf inside}}$ on the inside surface of the wall.

For the heating by solar walls, the thermal flux Φ_{o} from the ventilated air layer to the dwelling and the thermal flux $\Phi_{\text{sf inside}}$ from the inside surface of internal wall to the heating room are the most important parameters. Therefore, we are going to study these parameters.

Since the solar flux enter directly into the chimney between the glazing and the massive wall of the classical wall, the temperature of the fluid between the glazing and the massive wall is directly influenced by the solar thermal radiation. And the thermal flow that is lost crosses directly the glazing towards the exterior. The amplitudes of the air mass flow, of the temperature T_{o} of the air in the upper vent and of the thermal flux Φ_{o} from the air layer to the dwelling are therefore bigger.

With the composite wall, the solar flux is absorbed by the massive wall, and then some of it crosses the massive wall, and finally enters the chimney between the massive wall and the insulating wall. The entering or lost flux crosses the massive wall. The massive wall, with its great heat capacity, induced a dephasing on the heat fluxes evolution. The amplitudes of the air mass flow, of the temperature T_{o} of the air at the top orifice and of the thermal flux Φ_{o} from the orifice to the room are then smaller. And the changes of the amplitudes are delayed. On sunny days, the thermal flux enters the dwelling continually at night by the air mass flow. On sunny days and during the first day when it is not very sunny (60th day), it heats again the room at night. But the classical wall cannot heat the room at the night.

Since the thermal resistance of the insulating wall is bigger than that of the massive wall, the amplitudes of the temperature of the inside surface of the internal wall $T_{\text{sf inside}}$ and of the flux from the inside surface of internal wall to the room $\Phi_{\text{sf inside}}$ are smaller in the composite wall.

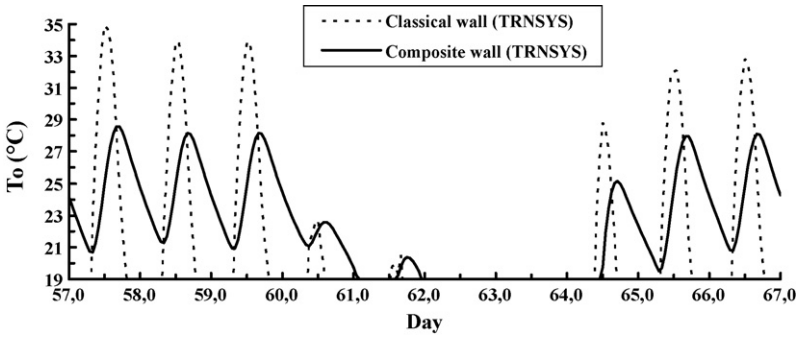

Fig. 20. Comparison of the temperatures T_{o} of the air at the upper vent of the wall.

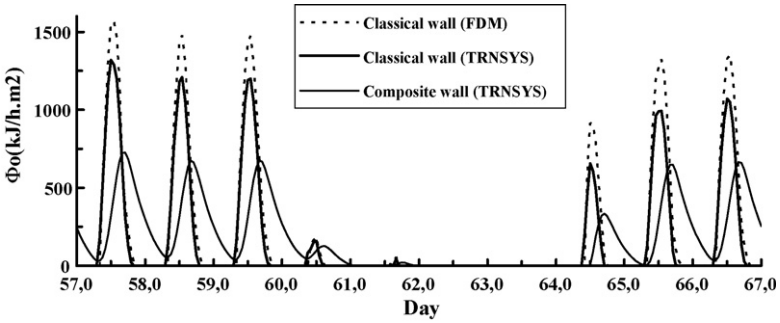

Fig. 21. Comparison of the thermal flux Φ_o from the ventilated air layer to the room.

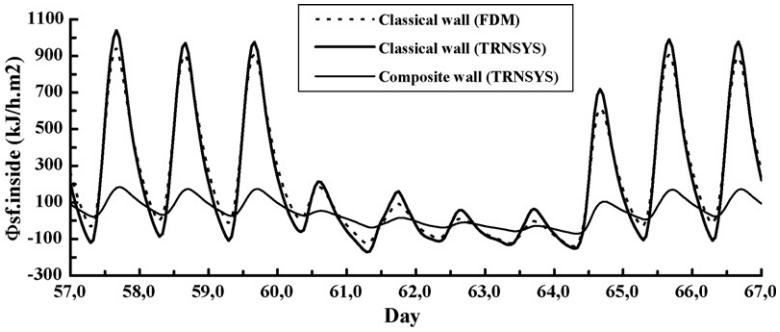

Fig. 22. Comparison of the thermal flux $\Phi_{sf\ inside}$.

7. Conclusion

The first part of our work consists in comparisons of the results obtained by our models and those obtained with a component (Type 36) of the TRNSYS library. This simulation program of transient thermal systems is well known. We find it often quoted as a reference in the specialized literature. The ''Type 36'' was adapted to our configuration (geometry, materials, etc.), and then the numerical simulations were carried out with meteorological data files that are very complete for the city of Carpentras. The obtained results show important discrepancies on certain magnitudes, and these discrepancies make obvious to carry out experimental studies associated to the construction of a model [1,4,5]. Certain approximations in the TRNSYS model (constant coefficients) make the results not very reliable.

In the second part that is the most important in our work, we created a new TRNSYS model (a ''type'') for a composite solar wall. This new model was compared with the results of simulation with the finite differences method that was validated by experimentation [4,5]. The results show that it is now a very interesting simulation tool which makes possible to study the performances and calculate the energy balance of this types of solar wall in comparison with simpler classical walls in various usage conditions.

References

[1] L. Zalewski, S. Lassue, B. Duthoit, M. Butez, Study of solar walls—validating a numerical simulation model, International Review on Building and Environment 37 (1) (2002) 109–121.

[2] Solar Laboratory of energy (USA), Manuals of TRNSYS, University of Wisconsin-Madison, USA, 1994.

[3] Z. Zrikem, E. Bilgen, Theoretical study of a composite Trombe–Michel wall solar collector system, Solar Energy 39 (5) (1987) 409–419.

[4] L. Zalewski, Etude thermique expérimentale et simulation numérique d'un mur solaire composite -Optimisation des performances énergétiques, Thèse de doctorat (PhD Thesis), Université d'Artois, Béthune, France, 1996.

[5] L. Zalewski, M. Chantant, S. Lassue, B. Duthoit, Experimental thermal study of a solar wall of composite type, Energy and Buildings 25 (1997) 7–18.

[6] K.G.T. Hollands, S.E. Unny, G.D. Raithby, L. Konicek, Free convective heat transfer across inclined air layers, Journal of Heat Transfer 98 (1976) 189.

[7] A.K. Sharma, et al., Vary-therm wall for cooling/heating of buildings in composite climate, International Journal of Energy Research 13 (1989) 733–739.

[8] W. Smolec, A. Thomas, Theoretical and experimental investigations of heat transfer in a Trombe wall, Energy Conversation Management 34 (5) (1993) 385–400.

[9] A.A. Sfeir, G. Guarracino, Ingénierie des systèmes solaires, applications à l'habitat, Technique et Documentation, 1981.

[10] J.F. Kreider, F. Kreith, Solar Energy Handbook, Mc Graw-Hill Series in Modern Structures, USA, 1981.

[11] W.H. Mc Adams, Heat Transmission, 3rd ed., McGraw-Hill, New York, 1954.

[12] P. Chouard, H. Michel et, M.F. Simon, Bilan thermique d'une maison solaire, Editions Eyrolles, Paris, 1977.

[13] J.A. Duffie, W.A. Beckman, Solar Engineering of Thermal Processes, John Wiley & Sons, New York, 1991.

[14] I.E. Idel'cik, Coefficients de pertes de charge singulières et de pertes de charge par frottement, Editions Eyrolles, 1979.

[15] M. Fishenden, O.A. Saunders, An Introduction to Heat Transfer, Oxford University Press, Oxford, 1950.

[16] 2001 ASHRAE Handbook, Fundamentals, SI Editions.